Journal of Alloys and Compounds 509 (2011) 5079–5083

Contents lists available at ScienceDirect

Journal of Alloys and Compounds

journal homepage: www.elsevier.com/locate/jallcom

High-frequency magnetic properties of $FeNi_3$–SiO_2 nanocomposite synthesized by a facile chemical method

Xuegang Lu*, Gongying Liang, Qianjin Sun, Caihua Yang

MOE Key Laboratory for Non-equilibrium synthesis and Modulation of Condensed Matter, School of Science, Xi'an Jiaotong University, Xi'an 710049, China

ARTICLE INFO

Article history:
Received 6 October 2010
Received in revised form 16 January 2011
Accepted 18 January 2011
Available online 22 January 2011

Keywords:
$FeNi_3$–SiO_2
Nanostructured materials
Chemical synthesis
Magnetic measurements
Magnetic properties

ABSTRACT

Monodisperse core–shell structured $FeNi_3$–SiO_2 composite nanoparticles (NPs) were synthesized by a facile hydrazine reduction combined modified Stöber method. SEM and TEM analysis shows that $FeNi_3$ cores are composed of small primary nanocrystals and are coated by amorphous SiO_2 layer. As-prepared $FeNi_3$–SiO_2 nanocomposites exhibit typical soft magnetic properties. The permeability spectra vary with the contents of SiO_2. When the SiO_2 content is 10 wt%, the real part μ' of the permeability reaches about 10 and is almost independent of frequency in the frequency range up to 1 GHz. And the imaginary part μ'' remains very low. This paper presents a facile approach to fabrication of novel soft magnetic materials for high-frequency applications.

1. Introduction

In the past decades, nanostructured magnetic materials have attracted intensive interest because of their excellent physical, catalytic, magnetic properties and their crucial applications in diverse fields, including catalysts [1], biomedical treatments and analysis [2], magnetic fluids [3], magnetic photonic crystals [4,5], high-density magnetic storage media [6,7], microwave absorbing materials [8–11], high-frequency soft magnetic materials [12–16]. In particular, the rapid developments of wireless communication devices have required miniature magnetic components, such as inductor and transformer, to be operated at high frequency. This requires that magnetic materials for high-frequency applications should have large saturation magnetization (M_s), high permeability μ' and low energy losses. However, none of the existing bulk magnetic alloys satisfy these requirements because of their low resistivity and large eddy-current loss. Soft magnetic ferrites have been traditionally used in high frequency applications because of their large permeabilities and low power losses. However, ferrites have an intrinsic disadvantage of small M_s. The high-frequency performance of these ferrites is limited by Snoek's law. Therefore, to meet these requirements, magnetic metal/insulator nanocomposites are frequently suggested to be used as materials for high-frequency applications [17–19]. By encapsulating magnetic metal nanoparticles with insulating phase, the resistivity of the materials can be dramatically increased. The eddy-current loss can be suppressed accordingly. Metal/insulator nanocomposites possess higher M_s. Moreover, the possible exchange coupling between neighboring nanoparticles can overcome the anisotropy and demagnetizing effects, thus resulting in much better soft magnetic properties than conventional materials [19].

Compared with traditional metals of Fe, Co and Ni, $FeNi_3$ alloy is proved to be a good candidate for soft magnetic materials due to its novel magnetic properties and thermal stability [20–23]. Coating $FeNi_3$ NPs with amorphous SiO_2 can effectively improve the electrical resistivity of the materials and suppress eddy-current losses in high-frequency operations [24]. Up to now, various methods have been developed to prepare magnetic alloy NPs and their nanocomposites [17–20]. However, most of them require rigorous conditions, such as high pressure, high temperature, inert atmosphere, vacuum, or H_2 atmosphere, which are inconvenient to operate in practice [25–34]. Recently, we reported a facile chemical method to synthesize $FeNi_3$ NPs in ambient air at low temperatures [35]. Based on this method, in this work monodisperse $FeNi_3$ NPs with hierarchic structures were prepared with the assistance of polyethylene glycol (PEG). Then, a modified Stöber method was employed to coat $FeNi_3$ NPs with a uniform amorphous SiO_2 layer. SiO_2 was chosen as the insulating phase because of its intrinsic high resistivity and stability. All the preparation was carried out in ambient air at room temperature. The structure and magnetic properties of this $FeNi_3$–SiO_2 nanocomposite were investigated.

* Corresponding author. Tel.: +86 29 87662390; fax: +86 29 87662630.
E-mail address: xglu@mail.xjtu.edu.cn (X. Lu).

0925-8388/$ – see front matter © 2011 Elsevier B.V. All rights reserved.
doi:10.1016/j.jallcom.2011.01.101

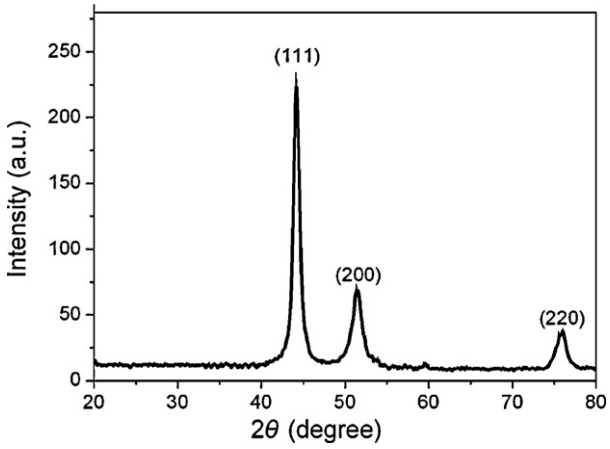

Fig. 1. XRD pattern of $FeNi_3$–SiO_2 NPs synthesized with $[N_2H_4{\cdot}H_2O]/[FeNi_3]$ ratio of 24:1.

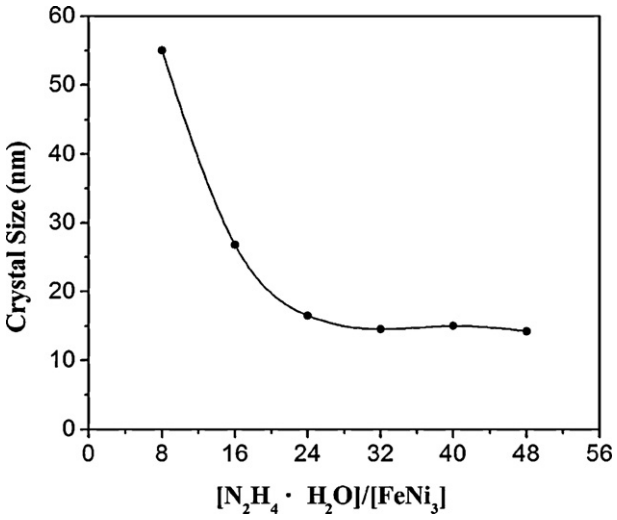

Fig. 2. Influence of $[N_2H_4{\cdot}H_2O]/[FeNi_3]$ ratios on the size of $FeNi_3$ crystals.

2. Experimental

2.1. Preparation of $FeNi_3$ NPs

$FeNi_3$ NPs were prepared using a wet chemical method similar to that of our previous work [35]. Different from previous work, PEG was used as surfactant agent in the process. The synthesis procedure is illustrated as follows: (1) 0.01 mol $FeCl_2{\cdot}4H_2O$ and 0.03 mol $NiCl_2{\cdot}6H_2O$ were dissolved into 200 mL distilled water, followed by the addition of PEG (1.0 g, MW 6000). (2) Sodium hydroxide (NaOH) was added to the solution and the pH value was controlled in the range $12 \leq pH \leq 13$. (3) Different amount of hydrazine hydrate ($N_2H_4{\cdot}H_2O$, 80% concentration) was added to the above suspension. The reaction was continued for about 24 h at room temperature. During this period, the pH value was adjusted by NaOH and kept in the range $12 \leq pH \leq 13$. The black $FeNi_3$ NPs were then rinsed several times with ionized water

2.2. Preparation of $FeNi_3$–SiO_2 nanocomposites

Core/shell $FeNi_3$–SiO_2 NPs were prepared according to the Stöber process with some modification. Typically, different amount of $FeNi_3$ NPs were dispersed in a mixture of 80 mL of ethanol, 20 mL of deioned water and 2.0 mL of 28 wt % concentrated ammonia aqueous solution ($NH_3{\cdot}H_2O$), followed by the addition of 0.20 g of tetraethyl orthosilicate (TEOS). After vigorous stirring for 24 h, the final suspension was repeatedly washed, filtered for several times and dried at 60 °C in the air.

2.3. Characterization of the nanocomposites

The crystal structure of the obtained particles was determined by powder X-ray diffraction (XRD) analysis using Cu Kα radiation. Morphology was analyzed using high-resolution transmission electron microscopy (HRTEM) on a JEOL-2010 transmission electron microscope operating at 200 kV. Elemental analysis was conducted using energy-dispersive X-ray spectroscopy (EDS) equipped on the field emission scanning electron microscopy (FE-SEM, JSM-7000F). Magnetic properties were studied using a Lake Shore vibrating sample magnetometer (VSM) with a maximum applied magnetic field of 10,000 Oe. The composite particles were compacted into rings at the pressure 12 ton/cm^2 for the permeability measurement. The size of the ring was 7 mm in outer diameter, 3 mm in inner diameter and 2 mm in thickness. Complex permeability spectra were measured in the range 1 MHz–1 GHz with a RF impedance/material analyzer (Agilent4291B + 16454A).

3. Results and discussion

Fig. 1 shows the XRD pattern of $FeNi_3$–SiO_2 nanocomposite particles synthesized with $[N_2H_4{\cdot}H_2O]/[FeNi_3]$ molar ratio of 24:1. It can be seen that three characteristic peaks for (FCC)-$FeNi_3$ ($2\theta = 44.3°$, 51.5°, 75.9°) from (1 1 1), (2 0 0) and (2 2 0) planes, are obtained. No XRD peaks for α-Fe (i.e. at 2θ of 65.2) and (FCC)-Ni (i.e. at 2θ of 44.5°, 51.8° and 76.4°) can be observed. In addition, no iron and nickel oxides or other impurity phases can be detected in the XRD patterns. The sharp and strong diffraction peaks confirm the good crystallization of the products. No crystalline SiO_2 is detected in all the samples, which reveals that SiO_2 phase in the $FeNi_3$–SiO_2 nanocomposite is in an amorphous state.

Normally, $N_2H_4{\cdot}H_2O$ can serve as either an oxidant or a reducer in alkali solution. Ni^{2+} can be easily reduced to Ni in alkali solution by $N_2H_4{\cdot}H_2O$. But for Fe^{2+}, it is difficult to be reduced to Fe directly by $N_2H_4{\cdot}H_2O$ because the electromotive force of oxidation reaction of Fe^{2+} to Fe^{3+} (0.66 V) is much larger than that of reduction reaction from Fe^{2+} to Fe (0.283 V). Thus, Fe^{2+} is more likely to be oxidized to Fe^{3+} when treated by $N_2H_4{\cdot}H_2O$ in alkali solution. In this experiment, however, when Fe^{2+} and Ni^{2+} coexist in the solution, Fe^{2+} ions can be easily reduced to Fe under the assistance of Ni^{2+} to form $FeNi_3$ alloy. The reduction reaction could be expressed as follows:

$$3Ni^{2+} + Fe^{2+} + 2N_2H_4 + 8OH^- \xrightarrow{pH\ 11-13} FeNi_3 + 2N_2 + 8H_2O \quad (1)$$

The size of $FeNi_3$ nanocrystals is dependent on the $[N_2H_4{\cdot}H_2O]/[FeNi_3]$ molar ratios and can be calculated with the Debye–Scherrer formula using X-ray line broadening theory. The influence of $[N_2H_4{\cdot}H_2O]/[FeNi_3]$ ratios on crystal size is illustrated in Fig. 2. The crystal size of $FeNi_3$ decreases with the increase of $[N_2H_4{\cdot}H_2O]/[FeNi_3]$ ratios and remains almost invariable (14 nm) when $[N_2H_4{\cdot}H_2O]/[FeNi_3]$ ratios are higher than 24:1.

Fig. 3 shows the SEM, HRTEM images and Energy-dispersive X-ray spectroscopy (EDS) spectrum of resultant $FeNi_3$ and $FeNi_3$–SiO_2 NPs. The $[N_2H_4{\cdot}H_2O]/[FeNi_3]$ ratio is 24:1 and the SiO_2 content is 10 wt%. The particle size of $FeNi_3$ determined by SEM (Fig. 3a) is in the range 50–80 nm, which is much larger than that estimated by XRD through Scherrer's equation. This indicates that resultant $FeNi_3$ particles have hierarchic structures, in which each large secondary $FeNi_3$ particle is composed of some smaller primary $FeNi_3$ nanoparticles or grains. This hierarchic structure can also be observed from the enlarged SEM image (inset) in Fig. 3a. From SEM (Fig. 3b) and TEM images (Fig. 3c and g), it can be seen that $FeNi_3$ NPs are uniformly coated by SiO_2 layer. Measuring the distance between two adjacent planes in a specific direction gives values of 0.205 nm and 0.355 nm (Fig. 3d), which correspond to the lattice spacing of (1 1 1) and (1 0 0) planes of (FCC)-$FeNi_3$. The selected-area electron diffraction (SAED) pattern taken from as-prepared $FeNi_3$–SiO_2 NPs consists of typical polycrystalline rings, suggesting a nanocrystalline structure. The diffraction peaks from (1 1 1), (2 0 0), (2 2 0), and (3 1 1) planes of (FCC)-$FeNi_3$ are totally in agreement with those of XRD. No diffraction peaks corresponding to crystalline SiO_2 are detected by TEM, indicating that the SiO_2 is

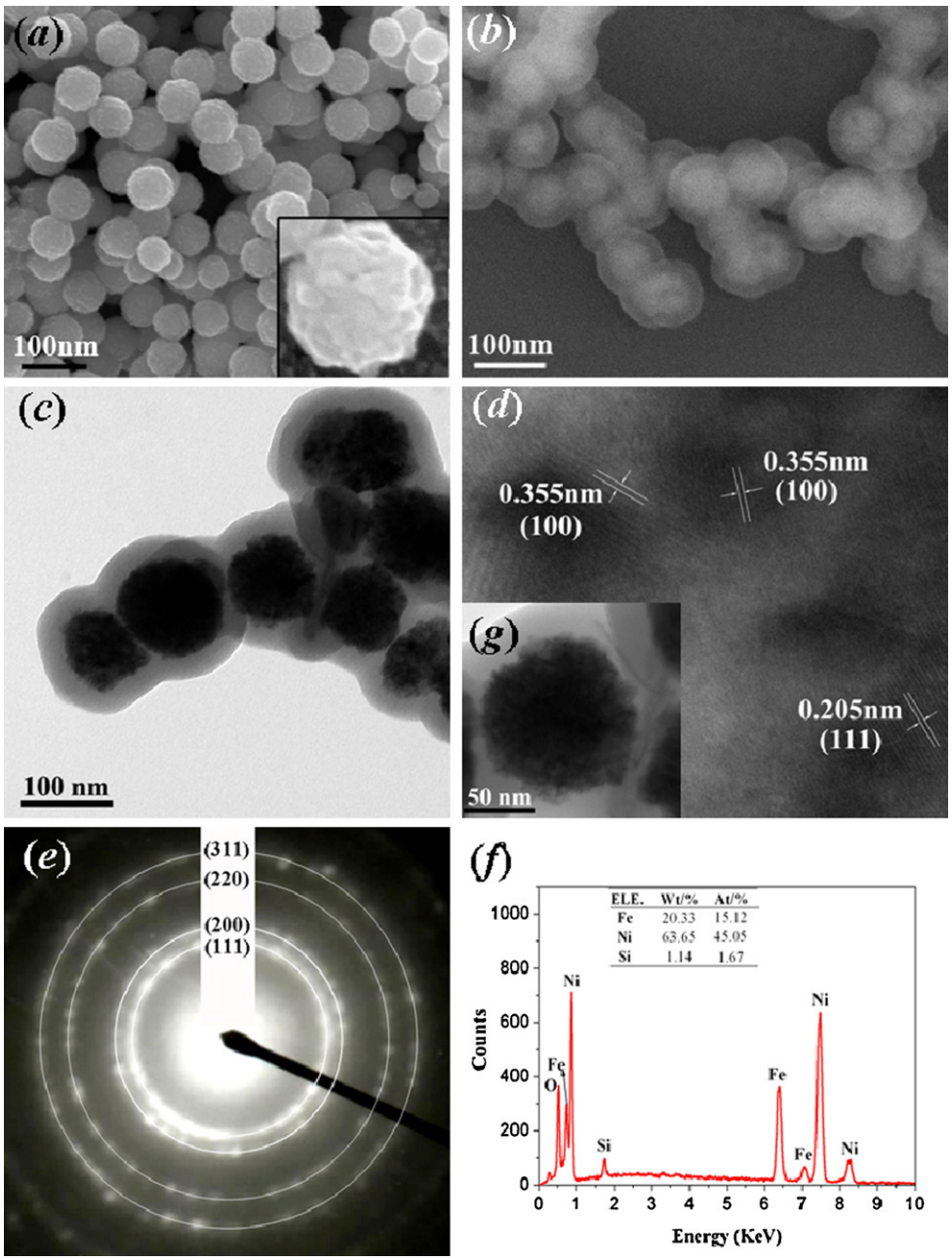

Fig. 3. Characterization of $FeNi_3$ and $FeNi_3$–SiO_2 NPs synthesized with 10 wt% SiO_2 and $[N_2H_4{\cdot}H_2O]$/[$FeNi_3$] ratio 24:1: (a) SEM image and enlarged SEM image (inset) of $FeNi_3$ NPs, (b) SEM image of $FeNi_3$ NPs coated by SiO_2, (c) HRTEM image of $FeNi_3$–SiO_2 NPs, (d) lattice fringe and (g) magnified image of $FeNi_3$–SiO_2 NPs, (e) SAED pattern of $FeNi_3$–SiO_2 NPs, (f) EDS result of $FeNi_3$–SiO_2 NPs.

amorphous. From EDS spectrum of $FeNi_3$–SiO_2 NPs (Fig. 3f), it is found that Fe, Ni and Si elements can be detected and the atomic ratio of Fe to Ni is 1:3. This further confirms that as-synthesized products are $FeNi_3$, not Ni.

The formation of hierarchic structure of $FeNi_3$–SiO_2 particles and bulk form of $FeNi_3$–SiO_2 nanocomposite can be illustrated by Fig. 4. First, primary $FeNi_3$ nanocrystals nucleate in solution with the assistance of hydrazine hydrate and PEG. Then surface modified $FeNi_3$ nanocrystals by PEG molecule chains aggregate into larger secondary particles. In the final step, $FeNi_3$ particles with hierarchic structure are coated with SiO_2 and are compacted into bulk form. Although PEG can not be directly observed in SEM and TEM images, we believed that PEG could be occluded in the SiO_2 shell and interface among primary $FeNi_3$ nanocrystals.

Fig. 5 shows the magnetic hysteresis loops for as-prepared $FeNi_3$–SiO_2 nanocomposites with different SiO_2 contents. It can be seen that $FeNi_3$–SiO_2 nanocomposites demonstrate typical soft magnetic characteristics. The M_s is 90 emu/g and the coercivity is 100 Oe for the $FeNi_3$–SiO_2 NPs with 10 wt% SiO_2. Meanwhile, the coercivity of compacted $FeNi_3$–SiO_2 samples is smaller than that of $FeNi_3$–SiO_2 NPs and decreases from 90 Oe to 20 Oe with the decrease of SiO_2 contents. The coercivity reduction for compacted $FeNi_3$–SiO_2 samples is believed to be due to the magnetic interactions between $FeNi_3$ nanocrystalls. For compacted bulk samples, dipolar interaction and/or exchange coupling among the nanoparticles leads to a reduction of the magnetic anisotropy and demagnetizing effects for each individual particle, so that the coercivity becomes smaller.

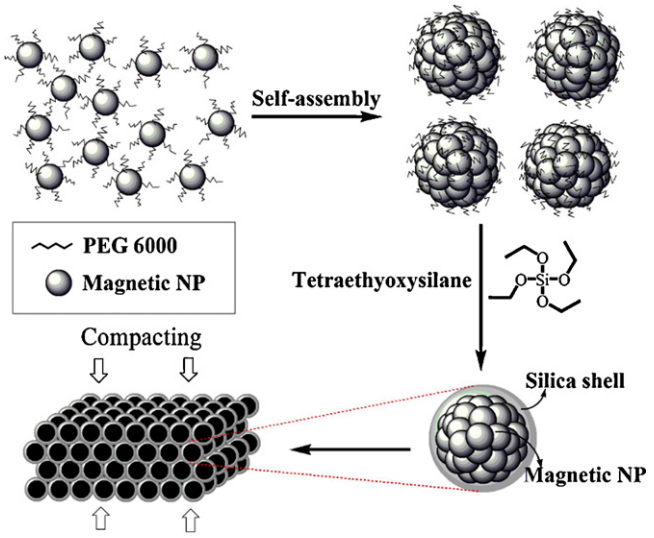

Fig. 4. Schematic illustration of the synthesis for $FeNi_3$–SiO_2 nanocomposite.

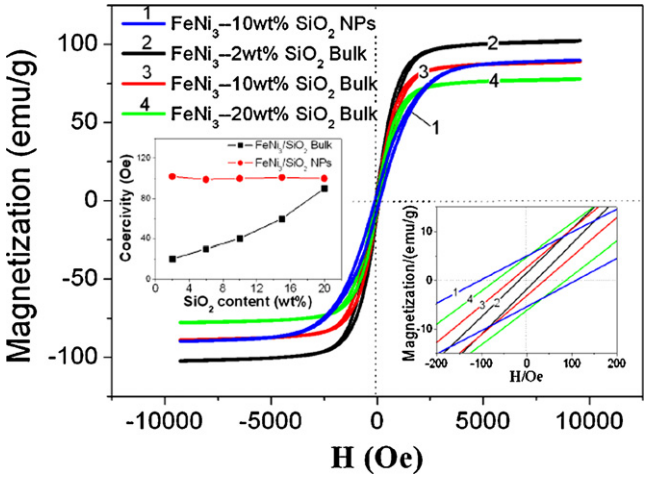

Fig. 5. Hysteresis loops for as-prepared $FeNi_3$–SiO_2 nanocomposite particles with different SiO_2 contents. The $[N_2H_4{\cdot}H_2O]/[FeNi_3]$ ratio is 24:1.

The frequency profile of the complex permeability ($\mu = \mu' - j\mu''$) for compacted $FeNi_3$–SiO_2 nanocomposite is measured and showed in Fig. 6. The SiO_2 contents are 2, 6, 10, 15 and 20 wt%, respectively. It is seen that the real part μ' of permeability decreases rapidly at low frequency range when the SiO_2 content is 2 wt%. When the SiO_2 content is increased to 6 wt%, the cut-off frequency is increased accordingly. With the further increase of SiO_2 content to above 10 wt%, a remarkable feature, in which the real part μ' of the permeability is almost independent of frequency up to at least 1 GHz, can be observed. These results demonstrate that the high-frequency magnetic properties of as-prepared $FeNi_3$–SiO_2 nanocomposites are superior to that of traditional $NiFe_2O_4$ or Co2Z type hexagonal ferrites. And most important, the properties of as-prepared $FeNi_3$–SiO_2 nanocomposites can be easily tuned through changing SiO_2 contents. This makes the materials usable in diverse fields of applications. Further experiments also show that size of $FeNi_3$ agglomerate spheres can be tuned from 100 nm to 180 nm by changing the reduction temperatures from 25 °C to 75 °C (see Fig. S1). However, no significant differences can be observed in the magnetic hysteresis loops for $FeNi_3$–SiO_2 nanocomposites with different size of $FeNi_3$ spheres (see Figs. S2–S4). When SiO_2 content is 15 wt%, the real part μ' of permeability for sample with 180 nm $FeNi_3$ cores is slightly higher than that with 100 nm $FeNi_3$ cores. And at the same time, the imaginary part μ'' of permeability is slightly increased.

This performance of the nanocomposites is attributed to the SiO_2 insulating phase. When the SiO_2 content is low, the insulation between $FeNi_3$ particles is poor so that large eddy-current loss is induced. As a result, the real part μ' of permeability decreases rapidly with the increase of frequency. With the increase of SiO_2 contents, the resistivity of the composite materials is improved so that the cut-off frequency is increased accordingly. Moreover, different from conventional magnetic powder materials, the eddy current loss produced within the particle is greatly diminished because the size of $FeNi_3$ NPs inside $FeNi_3$–SiO_2 nanocomposite is much smaller than that of eddy current skin depth [16].

In addition, due to the small size of $FeNi_3$ nanocrystals, the traditional domain-wall resonance may be absent or shift drastically upward in frequency. This is one of the reasons why $FeNi_3$–SiO_2 nanocomposite materials possess very high cut-off frequencies. Moreover, for the size of $FeNi_3$ nanocrystals (14 nm) is much smaller than the exchange length, l_{ex} ($l_{ex} \approx 154$ nm), the exchange coupling between $FeNi_3$ nanocrystals may take place [36]. This leads to a reduction of the magnetic anisotropy for each individual particle and the permeability of such nanocomposite is improved. In this work, the density of the nanocomposite is 89% of the ideal density. By increasing the density of the nanocomposites and selecting the appropriate SiO_2 shell thickness, the permeability in these materials may be further increased.

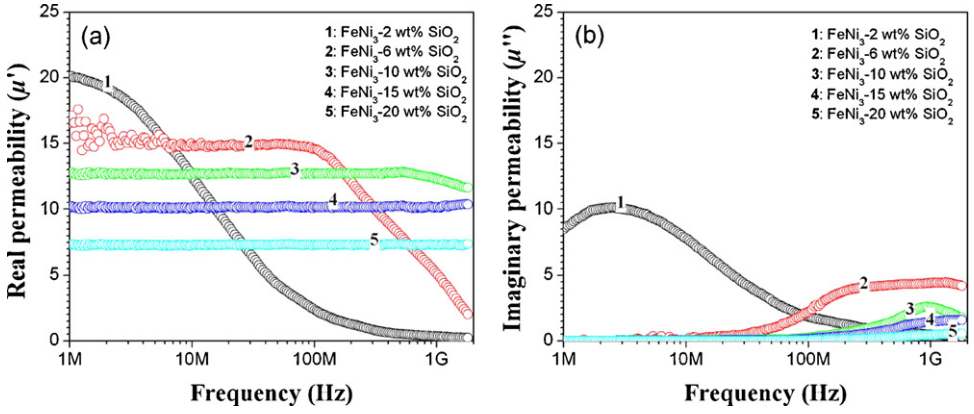

Fig. 6. Frequency dependence of the real (a) and imaginary (b) parts of the initial complex permeability, $\mu = \mu' - j\mu''$, for $FeNi_3$–SiO_2 nanocomposites sample.

4. Conclusions

In summary, we have successfully fabricated $FeNi_3$–SiO_2 nanocomposite using a facile hydrazine reduction combined modified Stöber method. (FCC)-$FeNi_3$ NPs with hierarchic structures were obtained with the assistance of polyethylene glycol (PEG). The crystal size is kept in the range 10–16 nm when the molar ratios of $[N_2H_4{\cdot}H_2O]$ to $[FeNi_3]$ are higher than 24:1. $FeNi_3$ particles coated by amorphous SiO_2 demonstrate typical soft magnetic properties. The cut-off frequency of the compacted sample increases with the increase of SiO_2 contents. The real part μ' of permeability remains almost unchanged up to at least 1 GHz when the SiO_2 contents are greater than 10 wt%. This method presents a promising route to produce high frequency soft magnetic materials.

Acknowledgements

We appreciate the financial support of the National Natural Science Foundation of China (no. 30772220) and New Teacher's Supporting Foundation of Xi'an Jiaotong University (no. 08141008).

Appendix A. Supplementary data

Supplementary data associated with this article can be found, in the online version, at doi:10.1016/j.jallcom.2011.01.101.

References

[1] J. Lee, Y. Lee, J.K. Youn, H.B. Na, T. Yu, H. Kim, S.M. Lee, Y.M. Koo, J.H. Kwak, H.G. Park, H.N. Chang, M. Hwang, J.G. Park, J. Kim, T. Hyeon, Small 229 (2008) 143.
[2] S. Gai, P. Yang, C. Li, W. Wang, Y. Dai, N. Niu, J. Lin, Adv. Funct. Mater. 20 (2010) 1166.
[3] H. Xia, J. Wang, Y. Tian, Q.D. Chen, X.B. Du, Y.L. Zhang, Y. He, H.B. Sun, Adv. Mater. 22 (2010) 3204.
[4] S. Pu, M. Liu, J. Alloys Compd. 481 (2009) 851.
[5] H. Kim, J. Ge, J. Kim, S. Choi, H. Lee, H. Lee, W. Park, Y. Yin, S. Kwon, Nature Photon. 3 (2009) 534.
[6] S. Sun, C.B. Murray, D. Weller, L. Folks, A. Moser, Science 287 (2000) 1989.
[7] Y. Luo, Y. Du, V. Misra, Nanotechnology 19 (2008) 265301.
[8] B.K. Kuanr, V. Veerakumar, K. Lingam, S.R. Mishra, A.V. Kuanr, R.E. Camley, Z. Celinski, J. Appl. Phys. 105 (2009), 07B522-1.
[9] X.G. Liu, Z.Q. Ou, D.Y. Geng, Z. Han, Z.G. Xie, Z.D. Zhang, J. Phys. D: Appl. Phys. 42 (2009) 155004–155011.
[10] X.G. Liu, B. Li, D.Y. Geng, W.B. Cui, F. Yang, Z.G. Xie, D.J. Kang, Z.D. Zhang, Carbon 47 (2009) 470.
[11] S. Ni, X. Wang, G. Zhou, F. Yang, J. Wang, D. He, J. Alloys Compd. 489 (2010) 252.
[12] X.G. Liu, D.Y. Geng, C.J. Choi, J.C. Kim, Z.D. Zhang, J. Nanopart. Res. 11 (2009) 2097.
[13] Y. Shirakata, N. Hidaka, M. Ishitsuka, A. Teramoto, T. Ohmi, IEEE Trans. Magn. 44 (2008) 2100.
[14] Y.W. Zhao, X.K. Zhang, J.Q. Xiao, Adv. Mater. 17 (2005) 915.
[15] Y. Shen, Z. Yue, M. Li, C.W. Nan, Adv. Funct. Mater. 15 (2005) 1100.
[16] L.Z. Wu, J. Ding, H.B. Jiang, C.P. Neo, L.F. Chen, C.K. Ong, J. Appl. Phys. 99 (2006) 083905–83911.
[17] S. Ohnuma, M. Ohnuma, H. Fujimori, T. Masumoto, J. Magn. Magn. Mater. 310 (2007) 2503.
[18] D. Yao, X. Zhou, H. Zuo, B. Zhang, Appl. Surf. Sci. 254 (2008) 2556.
[19] E. Thirumal, D. Prabhu, K. Chattopadhyay, V. Ravichandran, Phys. Status Solidi A 207 (2010) 2505.
[20] J. Jia, J.C. Yu, Y.X.J. Wang, K.M. Chan, ACS Appl. Mater. Interfaces 2 (2010) 2579.
[21] L. Zhen, Y.X. Gong, J.T. Jiang, W.Z. Shao, J. Appl. Phys. 104 (2008) 034312–34321.
[22] W. Gasior, Z. Moser, A. Debski, J. Alloys Compd. 487 (2009) 132.
[23] X.G. Liu, Z.Q. Ou, D.Y. Geng, Z. Han, J.J. Jiang, W. Liu, Z.D. Zhang, Carbon 48 (2010) 891.
[24] N.J. Tang, W. Zhong, H.Y. Jiang, Z.D. Han, W.Q. Zou, Y.W. Du, Solid State Commun. 132 (2004) 71.
[25] Z. Wang, X. Liu, M. Lv, J. Meng, Carbon 48 (2010) 3182.
[26] L.H. Bac, Y.S. Kwona, J.S. Kim, Y.I. Lee, D.W. Lee, J.C. Kim, Mater. Res. Bull. 45 (2010) 352.
[27] H. Wu, C. Qian, Y. Cao, P. Cao, W. Li, X. Zhang, X. Wei, J. Phys. Chem. Solids 71 (2010) 290.
[28] K.H. Kim, B.T. Lee, C.J. Choi, J. Alloys Compd. 491 (2010) 391.
[29] N.A.M. Barakat, K.A. Khalil, I.H. Mahmoud, M.A. Kanjwal, F.A. Sheikh, H.Y. Kim, J. Phys. Chem. C 114 (2010) 15589.
[30] C. Wang, R. Lv, Z. Huang, F. Kang, J. Gu, J. Alloys Compd. 509 (2011) 494.
[31] M.J. Hu, B. Lin, S.H. Yu, Nano. Res. 1 (2008) 303.
[32] M. Wen, Y.F. Wang, F. Zhang, Q.S. Wu, J. Phys. Chem. C 113 (2009) 5960.
[33] D.L. Peng, Y. Chen, H. She, R. Katoh, K. Sumiyama, J. Alloys Compd. 469 (2009) 276.
[34] L.P. Zhu, H.M. Xiao, S.Y. Fu, Eur. J. Inorg. Chem. (2007) 3947.
[35] X. Lu, G. Liang, Y. Zhang, Mater. Sci. Eng. B 139 (2007) 124.
[36] M.E. Mchenry, D.E. Laughlin, Acta Mater. 48 (2000) 223.